Characterization and mitigation of rf knockout during beam stacking

C. Jolly,[1,2] D. J. Kelliher,[1] J.-B. Lagrange,[1] A. P. Letchford,[1] S. Machida,[1] D. W. Posthuma de Boer,[1,2] C. T. Rogers,[1] and A. Seville[1]

[1]*STFC ISIS Department, Rutherford Appleton Laboratory, Harwell Campus, Didcot, OX11 0QX United Kingdom*

[2]*John Adams Institute for Accelerator Science, University of Oxford, Denys Wilkinson Building, Keble Road, Oxford, OX1 3RH, United Kingdom*

(Received 1 December 2025; revised 13 May 2026; accepted 5 May 2026; published 30 July 2026)

Beam stacking allows a fixed field alternating gradient accelerator (FFA) to increase the extracted beam current while also enabling a flexible time structure, making FFAs a promising candidate for future spallation neutron sources and other high intensity beam applications. For successful beam stacking, beam loss caused by rf knockout must be prevented. rf knockout can occur during beam stacking because of the finite dispersion function at the rf cavity location, which is unavoidable in a scaling FFA. In this work, the rf knockout resonance is characterized and through a series of experiments at the ISIS Neutron and Muon Source, we show that it is possible to suppress losses due to rf knockout.

DOI: 10.1103/nt4f-3cfm

I. INTRODUCTION

Beam stacking is one of the key advantages of fixed field alternating gradient accelerators (FFAs) for high intensity applications and could be a crucial technique in an FFA-based spallation neutron source [1]. With stacking, the beam can approach the space-charge limit at the extraction energy, allowing for a highly intense single pulse with greater flexibility in the time structure when compared with conventional synchrotron designs.

First achieved at MURA [2], beam stacking was later systematically demonstrated at Kyoto University's KURNS FFA [3]. While two beams were successfully stacked at the KURNS FFA, significant beam loss was observed during the stacking process. An rf program for beam stacking is shown in Fig. 1. During stacking, the first beam is injected and accelerated as usual. The beam is then debunched and stored as a coasting beam at the extraction energy. A second beam is then injected and accelerated. In this phase, the second beam (shown in orange in Fig. 1) is accelerated while the first beam is stored. Finally, the second beam is brought to an energy just less than that of the first beam and debunched, leaving two coasting beams that can now be thought of as a single stacked beam.

In a scaling FFA, the dispersion function is finite all around the ring so that the orbits of different momenta become photographic enlargements. Crucially, when a particle in the stored beam passes a cavity and gains or loses energy, the position of the equilibrium orbit changes to correspond to the new momentum. Since the particle is now offset with respect to the new equilibrium orbit, this causes a change in the betatron oscillation amplitude. Since the stored beam is not synchronized with the accelerating rf field of the second beam during stacking, the displacements nominally average out to zero.

However, when the rf frequency—which determines the frequency of the displacement—synchronizes with the phase advance of a betatron oscillation between cavities, the displacements could build up turn-by-turn, in a similar fashion to a transverse integer resonance.

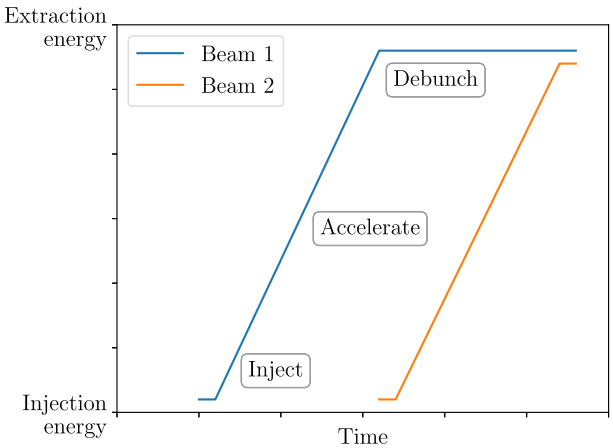

FIG. 1. An example rf beam stacking program with linear rf ramps. At the end of this program, two coasting beams will have been stacked at the extraction orbit.

Published by the American Physical Society under the terms of the Creative Commons Attribution 4.0 International license. Further distribution of this work must maintain attribution to the author(s) and the published article's title, journal citation, and DOI.

This effect is known as rf knockout and is consistent with the cause of beam loss during the beam stacking demonstration experiment at the KURNS FFA in 2023 [3]. The loss from rf knockout must be avoided for beam stacking to be a viable technique at a high intensity FFA. In this work, rf knockout is characterized and mitigation methods are tested experimentally at the ISIS Neutron and Muon Source [4].

II. RF KNOCKOUT

A. rf knockout mechanism

rf knockout is an external perturbation to a beam circulating in an accelerator. For example, a transverse rf field with a certain frequency can excite a coherent transverse beam oscillation when driven at the betatron frequency. An rf cavity can be a source of rf knockout when it is placed at a location with a finite dispersion function.

In a scaling FFA [5–7], the equilibrium orbit radius is determined by the momentum,

$$\frac{r_0+\delta x}{r_0}=\left(\frac{p_0+\delta p}{p_0}\right)^{\frac{1}{k+1}}, \tag{1}$$

where r_0 is the machine radius, p_0 is the beam momentum (the zero subscript indicates a reference value), k is the geometric field index, δx and δp are the changes in horizontal position and beam momentum, respectively. Taking the derivative of Eq. (1) gives the dispersion function, D_x, in a scaling FFA;

$$D_x=\frac{r_0}{k+1}.$$

An increase in particle energy at the rf cavities suddenly moves the equilibrium orbit. The magnitude of the displacement is proportional to the energy change, δE, and the dispersion function at the cavity,

$$\delta x=-\frac{\gamma D_x}{1+\gamma}\frac{\delta E}{E}.$$

Where γ is the Lorentz factor and E is the kinetic energy. The minus sign indicates that the closed orbit position moves, not the orbit.

The displacement due to a single rf cavity per crossing is a function of time.

$$\begin{aligned}\delta x(t)&=-\frac{\gamma D_x}{1+\gamma}\frac{V_{\mathrm{rf}}\sin(\omega_{\mathrm{rf}}t+\phi)}{E}\sum_{j=-\infty}^{\infty}\delta\left(\frac{t}{T_{\mathrm{rev}}}-j\right)\\&=-\frac{\gamma D_x}{1+\gamma}\frac{V_{\mathrm{rf}}\sin(\omega_{\mathrm{rf}}t+\phi)}{E}\sum_{n=-\infty}^{\infty}e^{in\omega_{\mathrm{rev}}t}\\&=\frac{i\gamma D_x V_{\mathrm{rf}}}{2(1+\gamma)E}\sum_{n=-\infty}^{\infty}\left(e^{i(\omega_{\mathrm{rf}}+n\omega_{\mathrm{rev}})t+i\phi}-e^{i(-\omega_{\mathrm{rf}}+n\omega_{\mathrm{rev}})t-i\phi}\right),\end{aligned} \tag{2}$$

where j is the turn index, t is time, T_{rev} is the revolution time, V_{rf} is the rf voltage, ω_{rf} is the cavity frequency, ϕ is the cavity phase offset, and i is the imaginary unit. n will be defined as the mode number at the end of this subsection.

The delta function is replaced by complex exponentials using a Fourier series.

A Hamiltonian for the beam equation of motion, including the displacements from rf knockout, can be constructed as,

$$H=\frac{p_x^2}{2m}+\frac{1}{2}m\omega_\beta^2x^2-\frac{\delta x}{T_{\mathrm{rev}}}p_x,$$

where m is the particle mass, p_x is the horizontal canonical momentum, ω_β is the betatron oscillation angular frequency. The equations of motion are;

$$\frac{dx}{dt}=\frac{\partial H}{\partial p_x}=\frac{p_x}{m}-\frac{\delta x}{T_{\mathrm{rev}}},$$

$$\frac{dp_x}{dt}=-\frac{\partial H}{\partial x}=-m\omega_\beta^2x,$$

and

$$\frac{d^2x}{dt^2}+\omega_\beta^2x=-\frac{1}{T_{\mathrm{rev}}}\frac{d\delta x}{dt}.$$

Therefore,

$$\begin{aligned}\frac{d^2x}{dt^2}+\omega_\beta^2x=&\frac{\gamma D_x V_{\mathrm{rf}}}{2(1+\gamma)ET_{\mathrm{rev}}}\\&\times\sum_{n=-\infty}^{\infty}\left(C_+e^{i(\omega_{\mathrm{rf}}+n\omega_{\mathrm{rev}})t}-C_-e^{i(-\omega_{\mathrm{rf}}+n\omega_{\mathrm{rev}})t}\right),\end{aligned} \tag{3}$$

and

$$\begin{aligned}C_+&=\left(\omega_{\mathrm{rf}}+n\omega_{\mathrm{rev}}\right)e^{i\phi},\\C_-&=\left(-\omega_{\mathrm{rf}}+n\omega_{\mathrm{rev}}\right)e^{-i\phi}.\end{aligned}$$

This will drive a betatron resonance when,

$$\omega_\beta=\pm\omega_{\mathrm{rf}}+n\omega_{\mathrm{rev}}. \tag{4}$$

By dividing through by the revolution frequency ω_{rev}, the rf knockout condition can be written in terms of the horizontal tune Q_x,

$$Q_x=\pm\frac{\omega_{\mathrm{rf}}}{\omega_{\mathrm{rev}}}+n.$$

The integer n can be interpreted as the mode number of the standing wave around the circumference, produced by rf knockout.

B. Amplitude growth from rf knockout

Following the analysis in [8], we derive the growth in the betatron amplitude due to rf knockout when the rf frequency is swept. We assume that the resonance condition of

Eq. (4) is satisfied at some point during ramping of the rf frequency. Regardless of the actual pattern of an rf frequency program, we can approximate that the rf frequency change is linear in time around the period when the resonance occurs;

$$\omega_{\mathrm{rf}}(t) = \omega_\beta - n\omega_{\mathrm{rev}} + \alpha t,$$

where α is the gradient of the linear frequency ramp. With a small phase difference of $\Omega(t)$ between betatron oscillations and the displacement,

$$\Omega(t_r) = \int_0^{t_r} \left[(\omega_{\mathrm{rf}}(t) + n\omega_{\mathrm{rev}}) - \omega_\beta\right] \mathrm{d}t = \int_0^{t_r} \alpha t \, \mathrm{d}t = \frac{\alpha}{2} t_r^2,$$

where t_r is defined with respect to the time when the resonance occurs.

In the vicinity of the resonance, one frequency component of Eq. (2) is added cumulatively every turn the beam passes an rf cavity.

$$\frac{d\delta x(t)}{dt} = \left(\frac{\omega_{\mathrm{rev}}}{2\pi}\right) \frac{i\gamma D_x V_{\mathrm{rf}}}{2(1+\gamma)E} e^{i\Omega(t)}.$$

The total displacement from the resonance crossing is;

$$\int_{-\infty}^{\infty} \frac{\mathrm{d}\delta x(t)}{\mathrm{d}t} \mathrm{d}t = \frac{i\gamma\omega_{\mathrm{rev}} D_x V_{\mathrm{rf}}}{4\pi(1+\gamma)E} \int_{-\infty}^{\infty} e^{i\Omega(t)} \mathrm{d}t = \frac{i\gamma\omega_{\mathrm{rev}} D_x V_{\mathrm{rf}}}{4\pi(1+\gamma)E} \sqrt{\frac{2\pi}{\alpha}} e^{i\pi/4}.$$

The absolute value gives the amplitude growth,

$$\Delta x = \left| \int_{-\infty}^{\infty} \frac{\mathrm{d}\delta x(t)}{\mathrm{d}t} \mathrm{d}t \right| = \frac{\gamma\omega_{\mathrm{rev}} D_x V_{\mathrm{rf}}}{4\pi(1+\gamma)E} \sqrt{\frac{2\pi}{\alpha}}. \quad (5)$$

From Eq. (5), the amplitude increase from passing through an rf knockout resonance is expected to vary linearly with voltage and the inverse square root of the crossing rate. We can arrive at a similar result by analogy with an integer resonance crossing. Baartman [9] and Le Duff [10] give equations with a similar form to Eq. (5), where the amplitude from an integer resonance crossing is linear with the magnetic field strength and the inverse square root of the crossing speed. With parameters used in the experiment section, e.g., $\gamma = 1.07$, $\omega_{\mathrm{rev}} = 0.675$ MHz, $D_x = 1.95$ m, $V_{\mathrm{rf}} = 10$ kV, $E = 70$ MeV, $\alpha = 5 \times 10^7$ MHz/s, the total displacement becomes $\Delta x = 17$ mm.

C. Mitigation methods

rf knockout mitigation methods were explored extensively at MURA [11,12]; here we review and test the mitigation methods experimentally.

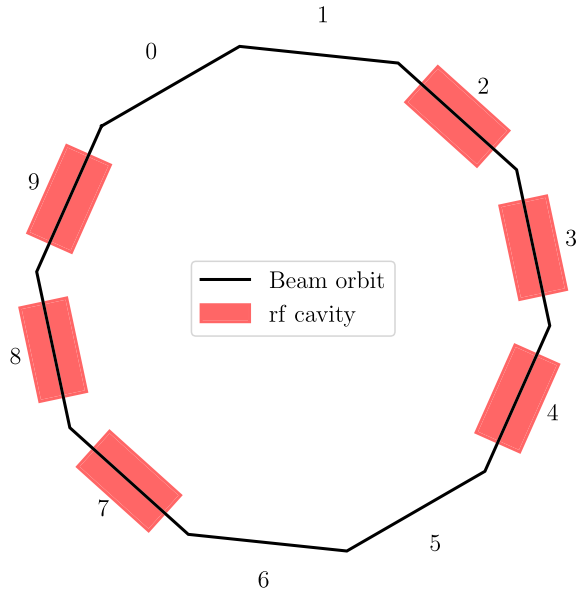

FIG. 2. A diagram of the fundamental (harmonic 2) rf cavity positions in the ISIS ring. The superperiods are numbered from 0 to 9. Each cavity is located at the same point in the superperiod.

The ISIS proton accelerator is conveniently arranged for testing rf knockout. ISIS's six fundamental (harmonic number $h = 2$) cavities are positioned in three consecutive superperiods in two groups on opposite sides of the ring [13]. The cavity arrangement is shown in Fig. 2. Crucially, the cavities are located at the same position in each cell so the dispersion function is the same at each cavity. By powering only some of the six cavities, several arrangements can be tested. In this study, we consider two cancellation methods, a local cancellation and a global cancellation of the rf knockout displacements.

1. Local cancellation

A sudden change in the equilibrium orbit due to the energy gain in the rf cavity and the finite dispersion function at the cavity can be canceled by other cavities located downstream.

We assume that the amplitude of the dispersion function at two cavities is the same and energy gains are the same as well. Figure 3 shows how rf knockout displacements could be canceled in a single turn by adjusting the relative amplitudes (a_1, a_2, and a_3) of three successive cavities. The three cavities are each separated by one superperiod. The phase advance from one cavity to the next is represented by ν_1 and ν_2. Starting from the origin, a particle experiences a displacement a_1 from the first cavity, then moves through a betatron phase advance, ν_1, to the next cavity, which has been set to a greater voltage. The particle experiences a correspondingly greater displacement from rf knockout. Finally, the particle moves through another phase advance, ν_2, to the final cavity, where it is given a

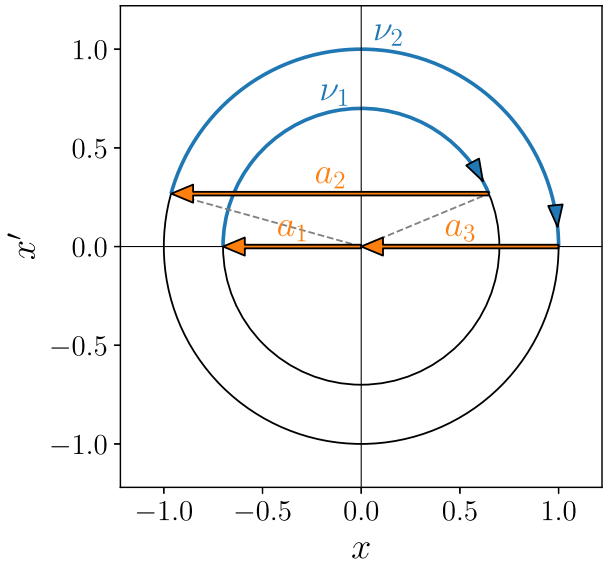

FIG. 3. A diagram showing how the displacements from rf knockout are canceled in a single turn using three successive cavities. a_1, a_2, and a_3 are the displacements at each cavity, ν_1 and ν_2 are the phase advances between the cavities.

final displacement a_3 to bring the particle back to the origin, thereby canceling the rf knockout displacements in a single turn.

An experimental test of mitigating rf knockout by locally canceling the displacements is discussed in Sec. III D 1.

2. Global cancellation with symmetric cavities

Following [8], we will derive the conditions for global correction. By adding an extra term, the driving force in Eq. (3) can be modified to account for M cavities spread throughout the ring. Writing the location of the mth cavity as θ_m, the azimuthal position with respect to a nominal fixed point is;

$$\theta_m = 2\pi \frac{L_m}{C},$$

where L_m is the cavity location in the ring and C is the ring circumference.

Equation (2) for M cavities is modified as

$$\delta x(t) = A \sum_{m=1}^{M} \sin\left(\omega_{\mathrm{rf}} t - h\theta_m + \phi\right) \times \sum_{j=-\infty}^{\infty} \delta\left(\frac{t}{T_{\mathrm{rev}}} - \frac{\theta_m}{2\pi} - j\right), \tag{6}$$

where A is the time independent constant of Eq. (2),

$$A = -\frac{\gamma D_x}{1+\gamma}\frac{V_{\mathrm{rf}}}{E},$$

h is the harmonic number of the rf system. The $h\theta_m$ term accounts for the rf phase delay between different cavity positions while the $\frac{\theta_m}{2\pi}$ term accounts for the extra kick the particle receives from the mth cavity.

Following the same procedure as the single cavity case, the driving force can be written as a sum of exponential functions:

$$\delta x(t) = \frac{iA}{2} \sum_{n=-\infty}^{\infty} e^{i(\omega_{\mathrm{rf}} + n\omega_{\mathrm{rev}})t + i\phi} \sum_{m=1}^{M} e^{-i\theta_m(h+n)}, - \frac{iA}{2} \sum_{n=-\infty}^{\infty} e^{i(-\omega_{\mathrm{rf}} + n\omega_{\mathrm{rev}})t - i\phi} \sum_{m=1}^{M} e^{-i\theta_m(-h+n)},$$

with the time dependent and independent terms separated into two exponentials.

The driving force from rf knockout will be zero when;

$$\sum_{m=1}^{M} e^{-i\theta_m(h+n)} = 0 \quad \text{for } \omega_\beta = \omega_{\mathrm{rf}} + n\omega_{\mathrm{rev}}, \tag{7}$$

$$\sum_{m=1}^{M} e^{-i\theta_m(-h+n)} = 0 \quad \text{for } \omega_\beta = -\omega_{\mathrm{rf}} + n\omega_{\mathrm{rev}}. \tag{8}$$

Consider two special cases: one with equally positioned rf cavities around the ring, and one with two cavities positioned with an azimuthal angle difference of $\Delta\theta$.

When multiple cavities are equally positioned around the ring, θ_m becomes;

$$\theta_m \to 2\pi \frac{m}{M}.$$

For this special case, Eq. (7) can be evaluated using the standard result for a geometric series;

$$\sum_{m=1}^{M} e^{-i2\pi \frac{m(h+n)}{M}} = \frac{1 - e^{-i2\pi(h+n)}}{1 - e^{-i2\pi \frac{(h+n)}{M}}}.$$

The sum is nonzero if;

$$\frac{h+n}{M} = p,$$

where p is a positive or negative integer. When this condition is satisfied,

$$\sum_{m=1}^{M} e^{-i2\pi \frac{m(h+n)}{M}} = M.$$

Therefore, the condition to avoid the rf knockout is,

$$\frac{h+n}{M} \neq p \quad \text{for } \omega_\beta = \omega_{\mathrm{rf}} + n\omega_{\mathrm{rev}}. \tag{9}$$

Similarly, from Eq. (8),

$$\frac{-h+n}{M} \neq p \quad \text{for } \omega_\beta = -\omega_{\mathrm{rf}} + n\omega_{\mathrm{rev}}. \tag{10}$$

It is clear that the number of knockout conditions is reduced proportionally to the number of rf cavities M.

TABLE I. $\pm\omega_{\rm rf}/\omega_{\rm rev}$ vs M. When $\frac{h+n}{M}$ or $\frac{-h+n}{M}$ is not an integer, rf knockout is mitigated. Otherwise, rf knockout occurs, indicated with bold values.

$\omega_{\rm rf}/\omega_{\rm rev}$	n	$M=1$	$M=2$	$M=3$	$M=4$
0.316	4	**6**	**3**	**2**	6/4
−0.684	5	**3**	3/2	**1**	3/4
1.316	3	**5**	5/2	5/3	5/4
−1.684	6	**4**	**2**	4/3	**1**
2.316	2	**4**	**2**	4/3	**1**
−2.684	7	**5**	5/2	5/3	5/4
3.316	1	**3**	3/2	**1**	3/4
−3.684	8	**6**	**3**	**2**	6/4
4.316	0	**2**	**1**	2/3	2/4
−4.684	9	**7**	7/2	7/3	7/4
5.316	−1	**1**	1/2	1/3	1/4
−5.684	10	**8**	**4**	8/3	**2**
6.316	−2	**0**	**0**	**0**	**0**
−6.684	11	**9**	9/2	**3**	9/4

Table I shows how the symmetrically positioned rf cavities suppress some of the rf knockout conditions in Eqs. (9) and (10). The parameters are based on the ISIS accelerator, where $Q_x = \omega_\beta/\omega_{\rm rev} = 4.316$ and $h = 2$.

When there are two cavities with the azimuthal angle difference of $\Delta\theta$, Eq. (7) becomes,

$$\sum_m e^{-i\theta_m(h+n)} = 1 + e^{-i\Delta\theta(h+n)}, \tag{11}$$

where we assume that the first cavity is positioned at a nominal fixed point $\theta_{m=1} = 0$ and the second cavity with an azimuthal position $\theta_{m=1} = \Delta\theta$. The condition to avoid the rf knockout is then,

TABLE II. $\pm\omega_{\rm rf}/\omega_{\rm rev}$ vs $\Delta\theta/2\pi$. When $\Delta\theta(h+n)/\pi$ or $\Delta\theta(-h+n)/\pi$ is an odd integer number, rf knockout is mitigated. Otherwise, rf knockout occurs, indicated with bold values.

$\omega_{\rm rf}/\omega_{\rm rev}$	n	$\Delta\theta/2\pi = 0.1$	0.2	0.3	0.4	0.5
0.316	4	**1.2**	**2.4**	**3.6**	**4.8**	**6**
−0.684	5	**0.6**	**1.2**	**1.8**	**2.4**	3
1.316	3	1	**2**	3	**4**	5
−1.684	6	**0.8**	**1.6**	**2.4**	**3.2**	**4**
2.316	2	**0.8**	**1.6**	**2.4**	**3.2**	**4**
−2.684	7	1	**2**	3	**4**	5
3.316	1	**0.6**	**1.2**	**1.8**	**2.4**	3
−3.684	8	**1.2**	**2.4**	**3.6**	**4.8**	**6**
4.316	0	**0.4**	**0.8**	**1.2**	**1.6**	**2**
−4.684	9	**1.4**	**2.8**	**4.2**	**5.6**	7
5.316	−1	**0.2**	**0.4**	**0.6**	**08**	1
−5.684	10	**1.6**	**3.2**	**4.8**	**6.4**	**8**
6.316	−2	**0**	**0**	**0**	**0**	**0**
−6.684	11	**1.8**	**3.6**	**5.4**	**7.2**	9

$$\Delta\theta(h+n) = \pm(2d-1)\pi \quad \text{for } \omega_\beta = \omega_{\rm rf} + n\omega_{\rm rev}, \tag{12}$$

$$\Delta\theta(-h+n) = \pm(2d-1)\pi \quad \text{for } \omega_\beta = -\omega_{\rm rf} + n\omega_{\rm rev}, \tag{13}$$

where d is an integer.

Table II shows the mitigated and unmitigated rf knockout conditions that satisfy Eqs. (12) and (13) for various positions of the second cavity.

III. MEASUREMENTS AT ISIS

A. Experimental setup

While beam stacking is only possible in fixed field machines, the effects of the beam stacking rf program can still be studied with the ISIS synchrotron. Key ISIS parameters relevant for the rf knockout experiments are given in Table III.

During normal operation, the magnetic field in the ISIS accelerator varies according to the beam's momentum. However, the machine can be set to a "storage ring mode," where the magnets produce a constant magnetic field at the field strength for the injection energy of roughly 70 MeV.

With a coasting beam stored at the ISIS injection momentum, a beam stacking rf program can be simulated by sweeping the rf frequency as if it were accelerating a second beam during stacking.

An example rf sweep is shown in Fig. 4. The program sweeps through nearly a whole rf harmonic to mimic the effect of the rf system accelerating a second incoming beam on a stored coasting beam during the beam stacking process.

Operating the rf program in Fig. 4 while a coasting beam is stored at the ISIS injection energy recreates the conditions during beam stacking in an FFA as shown in Fig. 1. However, it is noted that the cavities will ramp through a frequency greater than the coasting beam revolution frequency. Whereas in the conventional beam stacking case the frequency of the accelerating second beam is less than that of the stored coasting beam. This difference will not affect the physics of the rf knockout; it only means that a different rf knockout condition will be encountered.

TABLE III. Relevant ISIS parameters for rf knockout in storage ring mode.

Injection energy	70 MeV
Injection revolution frequency	0.675 MHz
Horizontal tune	4.316
Dispersion at $h = 2$ cavities	1.95 m
Operational beam intensity	$\sim 2.5 \times 10^{13}$
Typical intensity in rf knockout experiments	$\sim 2 \times 10^{12}$
Incoherent space-charge tune shift	~ -0.01

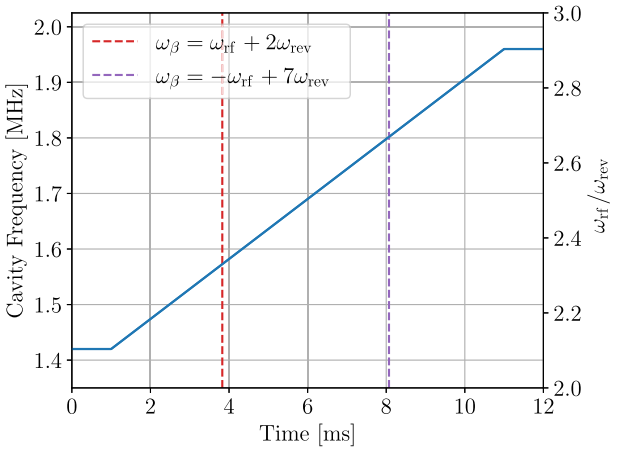

FIG. 4. An example radio frequency cavity program used to study rf knockout at ISIS. In this example, the cavity frequency ramps from 1.42 to 1.96 MHz or 2.1 to 2.9 times the coasting beam revolution frequency. The rf knockout conditions ($n = 2$ and $n = 7$) in this frequency range are indicated by the dashed lines.

The rf program ramps from 2.1 to 2.9 times the coasting beam revolution frequency. This range is within the normal operating parameters of the ISIS cavities and therefore ensures that the voltage across the cavity gap is as stable as possible over the ramp.

B. Confirmation of rf knockout

The current of the coasting beam was recorded while running the rf ramp shown in Fig. 4.

In this particular frequency range, there are two frequencies where the condition for rf knockout is met and two corresponding drops in the beam current, as shown in Fig. 5.

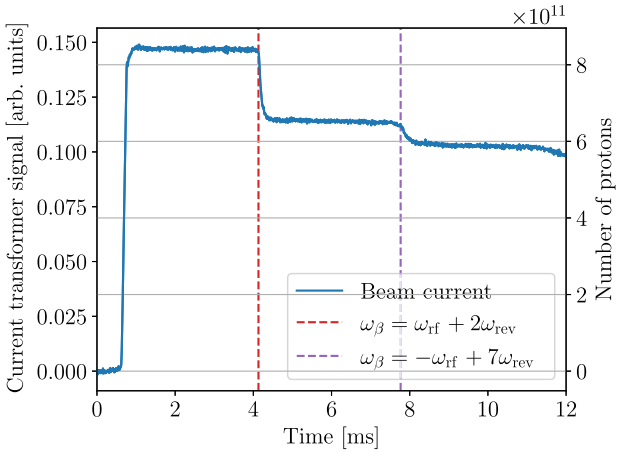

FIG. 5. Beam current showing loss resulting from two rf knockout resonances.

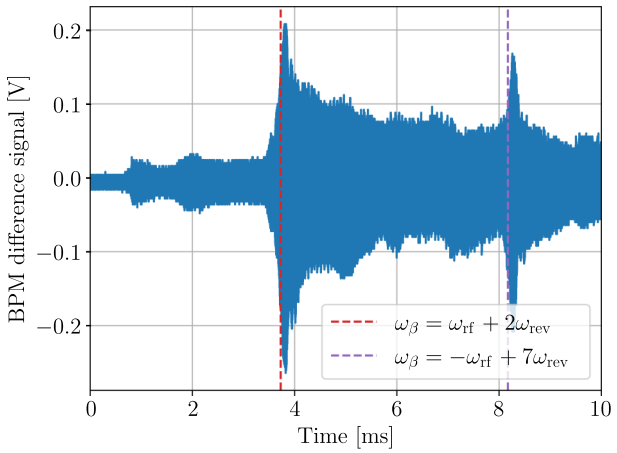

FIG. 6. Difference signal from a horizontal beam position monitor during a 10 ms rf ramp between 1.42 and 1.96 MHz. The beam's revolution frequency was 0.675 MHz. The rf passes through two rf knockout conditions at 4 and 8 ms resulting in an increase in betatron oscillation amplitude.

The displacement given to the beam during rf knockout can be seen with a beam position monitor (BPM). The ISIS BPMs consist of two capacitive pickups above and below the beam for a vertical position monitor and to the inside and outside of the ring for a horizontal monitor.

When the beam experiences a large displacement from rf knockout, the resulting horizontal betatron oscillation can be seen on the BPM difference signal. Figure 6 shows the BPM difference signal over a 10 ms rf ramp. There are two increases in amplitude at approximately 4 and 8 ms, indicating a large kick to the beam when the rf knockout condition is satisfied.

Since the beam remains unbunched throughout the rf ramp, there is no discernible signal on the sum signal of the two BPM plates. Therefore, it is not possible to measure an absolute position variation of the beam centroid from rf knockout. However, the difference signal can still be used to infer a relative change in beam position and quantify an increase in beam amplitude.

Figure 7 shows a spectrogram of the BPM difference signal for a 4 ms rf ramp. When the rf knockout condition is met, a betatron oscillation begins at the rf knockout frequency, the betatron oscillation also appears as sidebands of the beam's revolution frequency.

C. Parameter dependence

The amplitude increase from passing through an rf knockout resonance is expected to vary linearly with the rf voltage and with the inverse square root of the crossing speed. To confirm that Eq. (5) holds true, the rf ramp time and rf voltage were scanned using the same experimental setup explained in Sec. III A.

For each ramp time and rf voltage, the BPM difference signal was acquired throughout the rf ramp. The amplitude

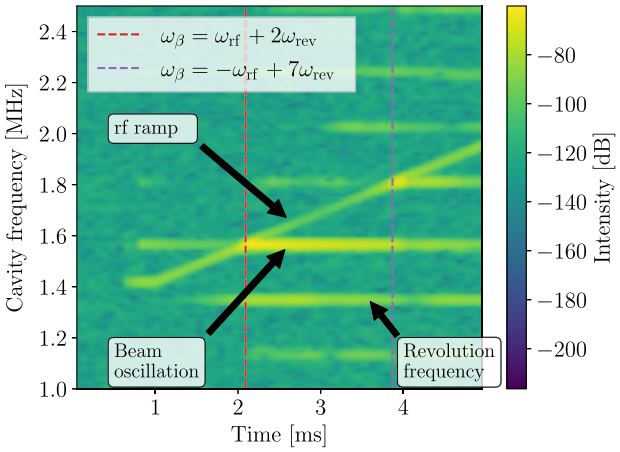

FIG. 7. Spectrogram of the difference signal from a beam position monitor during rf knockout. The revolution frequency and betatron oscillation caused by the rf knockout displacements are labeled. The rf cavity induces noise on the beam position monitor, which can be seen in the spectrogram.

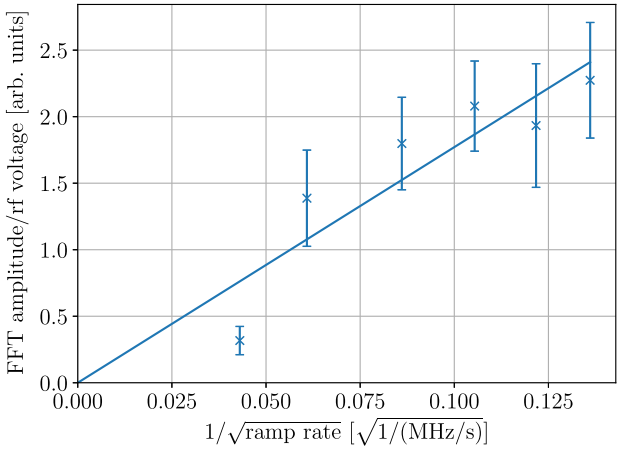

FIG. 9. Amplitude of the betatron oscillation vs $1/\sqrt{\text{ramp rate}}$ of the rf ramp. The data have been scaled according to the rf voltage applied.

of the betatron oscillation excited by passing through the rf knockout resonance was quantified by taking the Fourier transform of the BPM difference signal. A digital bandpass filter was then applied to isolate a specific harmonic of the betatron oscillation. The height of the peak was taken as a relative measurement of the change in beam amplitude from passing through the resonance.

The change in beam amplitude as measured from the Fourier transform is shown in Fig. 8. The linear fit includes both the horizontal and vertical error bars.

The error in the oscillation amplitude is the standard error on the mean of three repeated measurements. The error on the rf gap voltage seen by the beam is estimated to be around 250 V.

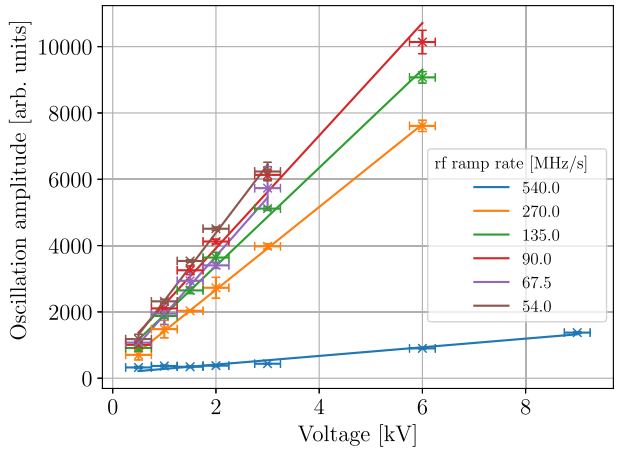

FIG. 8. Relative amplitude change of the beam after passing through an rf knockout resonance for various rf ramp rates. The betatron oscillation amplitude is expected to vary linearly with the cavity voltage.

In the 540 MHz/s ramp case, the line is a poorer fit to the data, as the fit is further from the estimated errors. Confidence in the model would be improved by taking additional repeats of this data but this was not possible with the limited machine time available.

From Eq. (5), the change in beam amplitude is also expected to vary according to the inverse square root of the rate of frequency change. Figure 9 shows the amplitude gain as a function of rf ramp time.

To assess whether the experimental data are consistent with Eq. (5), the data are plotted as amplitude vs $1/\sqrt{\text{ramp rate}}$ in Fig. 9. Similarly to Fig. 8, the error in the rf gap voltage is assumed to be 250 V. The data should follow a linear relationship, with the gradient of the line representing the constant term in Eq. (5). Unfortunately, the numerical value of the constant term cannot be cross checked with the gradient of the fit as the beam position measurement is relative.

Fitting a line to the logarithm of the betatron amplitude vs the logarithm of the ramp rate allows for the calculation of the exponent of the gradient, α in Eq. (5). The fit to the log data implies an exponent of -0.78 rather than the -0.5 expected from an inverse square root relationship. More repeats are needed to conclude that the amplitude varies with the inverse square root of the ramp rate.

Only data for which there was no significant beam loss is shown in Figs. 8 and 9. If the beam intensity changes significantly as a result of the rf knockout then that will affect the amplitude measurement. To make sure only beams of similar intensity are compared, any datasets with clear beam loss on the current monitor are excluded. Significant loss appeared for ramp times of 2 ms or greater for voltages larger than 6 kV. For the 6 and 10 ms ramp times, only data up to 3 kV was included.

D. Mitigation test

For beam stacking to be a viable technique in a high intensity FFA, beam loss due to rf knockout must be mitigated or avoided completely. In a ring with a single cavity, no mitigation or cancellation is possible.

As introduced in Sec. II, some of the resonance lines can be canceled by placing cavities symmetrically throughout the ring. Alternatively, rf knockout can be mitigated by locally canceling the displacements over a single turn. Here, both schemes are tested and compared experimentally.

1. Local cancellation with three cavities

The diagram in Fig. 3 is exaggerated for clarity; in the ISIS case, the two arc segments lie on the same radius and the angle between the vertical axis and the two dashed lines will be equal.

The rf cavity gap voltages required to cancel rf knockout can be calculated using the diagram. When $\nu_1 = \nu_2$, the amplitudes of the three cavities are related by;

$$\begin{aligned} &a_2 = 2a_1\cos(\nu); \quad \text{where,} \\ &a_1 = a_3 \quad \text{and} \quad \nu = \nu_1 = \nu_2. \end{aligned} \tag{14}$$

For the phase advance between adjacent cavities in the ISIS ring, this leads to a voltage ratio across the three cavities of 0.55 : 1.0 : 0.55. To confirm that this mitigation strategy works in practice, this voltage ratio was applied to three of the ISIS cavities in consecutive superperiods. Otherwise, the experimental setup was similar to Sec. III A and the same frequency sweep shown in Fig. 4 was used. The effect of the mitigation strategy on the coasting beam current is shown in Fig. 10. The beam loss caused by rf knockout is completely eliminated to within the minimum sensitivity of the current transformer.

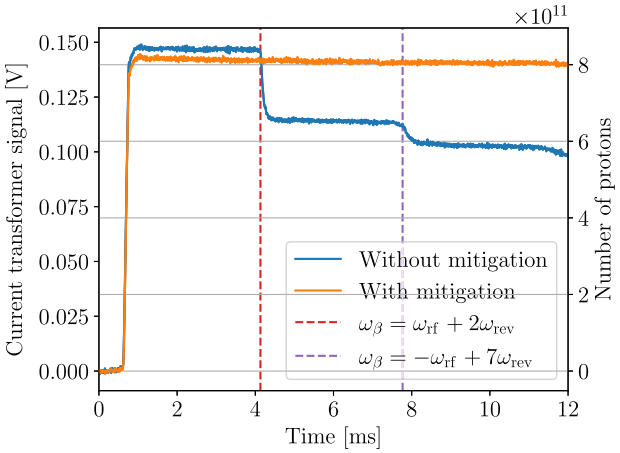

FIG. 10. Beam current without and with the local cancellation mitigation method.

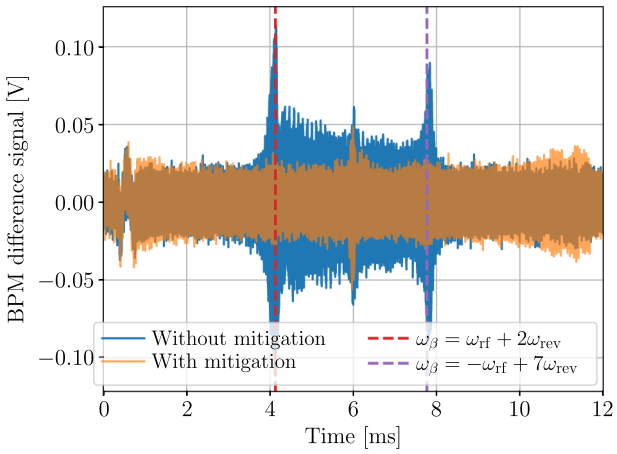

FIG. 11. Beam position monitor difference signal without and with the local cancellation mitigation method. Both rf knockout conditions are suppressed by canceling the displacements in a single turn with three successive cavities.

Although there was no observable beam loss with this mitigation strategy, the beam may still have received a kick from the rf knockout resonance; if present, the kick should be visible in the BPM difference signal. Figure 11 shows the BPM difference signals, with and without the mitigation strategy, overlaid. In the unmitigated rf knockout, the betatron oscillation can be seen at the two points where the rf knockout condition was met. In the data with mitigation, there is no identifiable oscillation indicating that the kick displacements were canceled as predicted in Fig. 3.

At around 6 ms in Fig. 11, a small peak appears in both the case with and without mitigation. The peak occurs exactly halfway through the rf ramp, when the rf frequency is 2.5 times the revolution frequency. The peak is the result of some transient bunching of the beam from the 5th harmonic of the rf frequency. The bunching quickly dissipates as the rf frequency moves past 2.5 times the revolution frequency.

2. Global cancellation with symmetric cavities

In the previous section, the loss from rf knockout was eliminated by canceling the displacements within a single turn. While the local cancellation method is effective, it is not a particularly practical option as the acceleration of the incoming beam is compromised to enable the mitigation of rf knockout.

The global cancellation method described in Sec. II C 2 does not affect the acceleration of the incoming beam and is independent of the phase offset between the cavities.

To test this mitigation method, the frequency ramp in Fig. 4 was applied using two cavities on exact opposite sides of the ISIS ring, delivering equal voltages. Figure 2 shows the position of the fundamental cavities in the ISIS ring. According to Eq. (11), in the special case of two

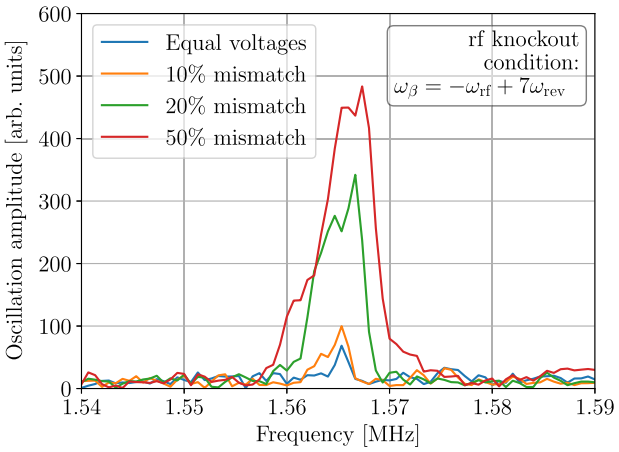

FIG. 12. Betatron oscillation from the rf knockout for a mode number of seven is reduced with two cavities delivering equal voltages on opposite sides of the ISIS accelerator. As the voltage mismatch between the cavities is increased, the rf knockout displacements are no longer canceled.

cavities on opposite sides of the ring, all odd numbered modes will be canceled. For the ISIS accelerator with its harmonic two rf system, the $n = 2$ mode will be unaffected but the $n = 7$ mode will be canceled. It is important to note that unlike the local cancellation method, the rf knockout displacements are not canceled out in a single turn. The odd number oscillations triggered by rf knockout are canceled because the symmetry of the cavity arrangement removes the rf knockout driving force.

The amplitude of the $n = 7$ oscillation for various cavity settings is shown in Fig. 12. With the two cavities set to equal voltages the oscillation induced by the rf knockout displacements is reduced, as shown by the blue line in Fig. 12. The voltage of one of the two cavities was then varied to deliver an unequal voltage to the beam. As the voltage mismatch increases, the symmetry is broken and the rf knockout kicks become more pronounced.

A detectable betatron oscillation persists even with the two cavities set to equal voltages. As the voltage mismatch increases, the beam approaches the single cavity case and the resulting betatron oscillation grows. The comparatively small betatron oscillation with the cavities set to equal voltages is likely caused by the error on the voltage delivered by the cavities. Although there was an induced oscillation, there was no measurable loss on the ISIS beam current monitor in the equal voltage case.

TABLE IV. ω_{rf}/ω_{rev} vs $\Delta\theta$ when $h = 2$. When $\Delta\theta(h+n)/\pi$ or $\Delta\theta(-h+n)/\pi$ is an odd integer number (shown in bold), the knockout does not occur.

ω_{rf}/ω_{rev}	n	$\Delta\theta/2\pi = 0.1$	0.2	0.3	0.4	0.5
2.316	2	**0.8**	**1.6**	**2.4**	**3.2**	**4**
−2.684	7	1	**2**	3	**4**	5

Global cancellation with symmetric cavity positioning does not necessarily impose two cavities on the opposite sides of a ring. That is only the special case of Eq. (11) when $\Delta\theta = \pi$. As shown in Fig. 2, the ISIS accelerator has a tenfold symmetry and the six rf fundamental cavities are installed at the identical position in each superperiod of no. 2, no. 3, no. 4, no. 7, no. 8, and no. 9. The combination of two cavities from different superperiods will yield the condition of $\Delta\theta/2\pi = 0.1, 0.2, 0.3, 0.4$, and 0.5. Table IV shows when the mitigation works for those combinations.

Figure 14 in Appendix A shows that the rf knockout of the $n = 7$ is suppressed when two cavities are separated by $\Delta\theta/2\pi = 0.1, 0.3$, or 0.5, as expected from Table IV.

IV. DISCUSSION

While the rf knockout mitigation schemes discussed in Sec. III D can prevent beam loss during stacking, both methods have drawbacks.

The local cancellation method cancels all rf knockout kicks but depends on the phase advance of the particle. It also compromises the accelerating rf program, as both the phase and voltage of the cavities must change to enable local cancellation. This requirement introduces additional complexity. rf knockout occurs in the stored coasting beam at the top energy of the FFA; therefore any mitigation strategy must avoid rf knockout in the stored beam while maintaining the acceleration of the incoming beam. Here, the accelerating voltage has already been reduced to cancel the rf knockout kicks; however, the cavities should be phased such that the beam receives the intended displacement from the cavity. This leads to a unique situation where the cavities need to be phased to perfectly cancel rf knockout while simultaneously maintaining acceleration of the incoming beam. It is not possible to achieve both simultaneously, so an imperfect phase setting must be used for either the acceleration or the mitigation.

To assess the sensitivity of the local cancellation to a phasing error, the experiment in Fig. 10 was repeated for a range of relative phases between the cavities. The cavity phase offset refers to the rf phase angle between successive cavities. Normally, when accelerating a beam that is synchronized with the rf waveform, the cavity phase offset is set equal to the rf phase angle between the cavities, 72°. During rf knockout, the cavity frequency is not synchronized with the stored beam therefore an adjusted phase offset should be used to ensure full cancellation of the displacements.

In this experiment, rf knockout occurs at cavity frequencies 2.313 ($n = 2$ mode) and 2.687 ($n = 7$ mode) times the revolution frequency. The cavity phase offset must be adjusted to account for the cavity frequency at which the rf knockout condition is met. The cavity phase offset is given by; $\frac{\omega_{rf}}{\omega_{rev}}\frac{2\pi}{N}$, where N is the number of superperiods (for ISIS, $N = 10$).

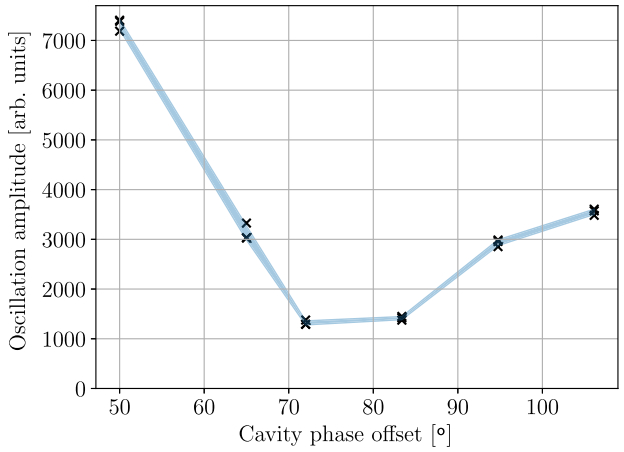

FIG. 13. Amplitude of the betatron oscillation triggered by rf knockout varies with a phasing error between cavities. Three repeats for each phase are shown. The shaded area indicates the standard error on the mean of the three repeats.

Taking the $n = 2$ rf knockout, a phase offset of roughly 83.3° matches the phase of rf to the beam at a cavity frequency of 2.313 times the revolution frequency. Then, the combination of the three cavities should cancel the rf knockout displacements perfectly. Figure 13 shows the effect of changing the cavity phase offset. As the phase moves away from the ideal value, the displacements are no longer canceled and an oscillation of the beam centroid can be detected.

Using Eq. (14) to calculate the cavity phase offset ν for the ISIS case—an 83.3° phase offset should perfectly cancel the rf knockout kicks and therefore prevent the amplitude growth from rf knockout. However, there is still a detectable oscillation at the horizontal tune frequency for the 83.3° offset.

Clearly, the rf knockout displacements were not completely canceled. The most likely cause of the persisting oscillation is the uncertainty in the rf voltages applied to the beam. The voltage produced at the cavity gap is accurate to around 250 V. Ideally, the rf voltage across the three cavities should follow the ratio 0.55∶ 1.0∶ 0.55, but in reality it is likely that this ratio was not quite achieved, leading to a detectable oscillation even when the cavities were phased perfectly.

The cable delays in the rf system were recently measured and adjusted; it is thought that the error in the rf waveform phase is small compared with the error on the voltage.

Unlike the local cancellation method, the global cancellation with symmetrical cavities is independent of the phase advance and does not compromise the accelerating rf program. Nevertheless, the global cancellation method has some disadvantages. It does not cancel every occurrence of rf knockout and requires specific cavity positions in the ring.

Beam stacking is particularly useful in a high intensity FFA [1,3]; collective effects associated with a highly intense beam could be present before, during, and after the stacking process. The rf knockout cancellation responds differently to a space-charge tune spread depending on the mitigation strategy.

In the local cancellation case, the elimination of rf knockout depends on the total displacements summing to zero in a single turn of the ring. The local cancellation method therefore depends on the phase advance of individual particles in the beam. In the high intensity scenario, the beam will have a space-charge tune spread, and the diagram in Fig. 3 will no longer apply exactly to every particle, as each particle's phase advance will be different and the effect of the local cancellation may be degraded.

The global cancellation by symmetric cavities mitigates some of the rf knockout kicks with a different principle. This method eliminates rf knockout by canceling the displacements from the cavities. Since this method does not rely on the phase advance of an individual particle it should be unaffected by a space-charge tune spread. We therefore consider that the global cancellation method is the best option for a high intensity FFA. In the experimental demonstration of the global cancellation, only two cavities were used. As a result, only the $n = 7$ mode was canceled and the $n = 2$ mode remained unmitigated. By incorporating more symmetrically places cavities, more rf knockout modes will be canceled. As long as the cavities are placed with the global cancellation of rf knockout in mind then more rf knockout modes will be canceled. For a high intensity beam, any unmitigated rf knockout modes would likely cause significant beam loss but with the number of cavities available in a full-scale FFA, the problematic mode(s) can be avoided. Furthermore, one of the suggested energy ranges for ISIS-II is 400 to 1200 MeV. While this energy range has an extraction momentum to injection momentum ratio of 2, the frequency ratio is only ≈ 1.26. At the design stage of an ISIS-II scale FFA, one must place the cavities symmetrically to produce the global cancellation of rf knockout in the rf frequency range of interest. With the number of cavities available in a full-scale FFA, we expect it will be possible to find an rf knockout free frequency range.

In the experimental studies of the local cancellation method, a low intensity coasting beam of around 2×10^{12} particles was used. The space-charge tune shift is almost nonexistent at this intensity as the beam is unbunched. During user cycles, ISIS operates at an intensity around 10 times greater, but it is difficult to store this intensity in storage ring mode at the injection energy. High intensity experimental studies are one avenue for future research.

V. CONCLUSION

rf knockout has been confirmed experimentally as the source of beam loss during beam stacking at the KURNS FFA. There are no dispersion free regions in a scaling FFA; therefore, for beam stacking to be a viable technique, the

beam loss from rf knockout must be mitigated. We have shown experimentally that rf knockout can be mitigated with two techniques: local and global cancellation. The local cancellation method can cancel all rf knockout displacements but could also compromise the acceleration of beams during stacking. While the global cancellation does not cancel all rf knockout oscillation modes, the global cancellation method can create an rf knockout free frequency range large enough for a beam stacking rf program to be executed without compromising beam acceleration. Furthermore, the global cancellation is independent of the particle tune making it a viable option for beam stacking at a high intensity FFA for a future Spallation Neutron Source.

ACKNOWLEDGMENTS

We wish to acknowledge the operations team of the ISIS accelerator, especially H. Cavanagh and the ISIS Crew. Thanks also to R. Williamson for his comments on the manuscript.

DATA AVAILABILITY

The data that support the findings of this article are openly available [14], embargo periods may apply.

APPENDIX A: RF KNOCKOUT MITIGATION WITH NONSYMMETRIC RF CAVITIES

Experimental results on the rf knockout mitigation by two rf cavities are shown here. Because of a tenfold symmetry of the ISIS lattice, it is possible to test various values of $\Delta\theta$ in Eqs. (12) and (13).

APPENDIX B: ASYMMETRY OF FIG. 13

The asymmetric behavior of Fig. 13 with respect to the minimum seems strange because the rf phase shift to either direction adds a residual oscillations and its amount is linear around the minimum. Starting with similar equations for the global cancellation of Eq. (6), we analyze how the quality of the local cancellation depends the phase offset between cavities. First, we substitute $\frac{\omega_{\rm rf}}{\omega_{\rm rev}}$ for h, which defines the required phase offset when the ratio is not an integer. The time from one cavity to the next is;

$$\Delta t = \frac{\Delta\theta}{2\pi} T_{\rm rev} = \frac{\Delta\theta}{\omega_{\rm rev}},$$

where $\Delta\theta$ is the angular distance between two cavities, the phase offset required for a particle to pick up the same phase at two cavities is,

$$\Delta\phi = \int_0^{\Delta t} \omega_{\rm rf}(t)\,{\rm d}t \simeq \frac{\omega_{\rm rf}}{\omega_{\rm rev}}\Delta\theta.$$

Second, we set A different for each cavity by A_m.

$$\delta x(t) = \sum_{m=1}^{M} A_m \sin\left(\omega_{\rm rf} t - \frac{\omega_{\rm rf}}{\omega_{\rm rev}}\theta_m + \phi\right) \times \sum_{j=-\infty}^{\infty} \delta\left(\frac{t}{T_{\rm rev}} - \frac{\theta_m}{2\pi} - j\right).$$

We separate time dependent and independent parts,

$$\delta x(t) = \frac{i}{2}\sum_{n=-\infty}^{\infty} e^{i(\omega_{\rm rf}+n\omega_{\rm rev})t+i\phi}\sum_{m=1}^{M} A_m e^{-i\theta_m\left(\frac{\omega_{\rm rf}}{\omega_{\rm rev}}+n\right)}, \quad -\frac{i}{2}\sum_{n=-\infty}^{\infty} e^{i(-\omega_{\rm rf}+n\omega_{\rm rev})t-i\phi}\sum_{m=1}^{M} A_m e^{-i\theta_m\left(-\frac{\omega_{\rm rf}}{\omega_{\rm rev}}+n\right)}.$$

We are interested in the mitigation when $\omega_\beta = \omega_{\rm rf} + n\omega_{\rm rev}$ so we consider the first term only. The amplitude of the first and the third cavities are lower than the second one by a factor of;

$$\frac{A_{1,3}}{A_2} = -\frac{1}{2\cos\nu} = -\frac{1}{2\cos\frac{2\pi Q_x}{10}},$$

where ν is a horizontal phase advance between cavities and equal to $Q_x/10$ because of the tenfold symmetry lattice. The time independent part with the local cancellation setting becomes

$$\sum_{m=1}^{3} A_m e^{-i\theta_m\left(\frac{\omega_{\rm rf}}{\omega_{\rm rev}}+n\right)} = -\frac{e^{i\frac{2\pi}{10}\left(\frac{\omega_{\rm rf}}{\omega_{\rm rev}}+n\right)}}{2\cos\frac{2\pi Q_x}{10}} + 1 - \frac{e^{-i\frac{2\pi}{10}\left(\frac{\omega_{\rm rf}}{\omega_{\rm rev}}+n\right)}}{2\cos\frac{2\pi Q_x}{10}} = 1 - \frac{\cos\frac{2\pi}{10}\left(\frac{\omega_{\rm rf}}{\omega_{\rm rev}}+n\right)}{\cos\frac{2\pi Q_x}{10}}, \tag{B1}$$

where n is an integer. This becomes zero when $n = 2$ and $\frac{\omega_{\rm rf}}{\omega_{\rm rev}} + 2 = Q_x$, as shown in Fig. 13. However, there is another $\frac{\omega_{\rm rf}}{\omega_{\rm rev}} + 2$, which makes the term zero when $\frac{\omega_{\rm rf}}{\omega_{\rm rev}} + 2 = 10 - Q_x$. Figure 15 from Eq. (B1) shows the residual oscillation amplitude depending on the phase offset. As a result of the two minima as a function of $\frac{\omega_{\rm rf}}{\omega_{\rm rev}}$, Fig. 13 is not symmetric with respect to one of the minima.

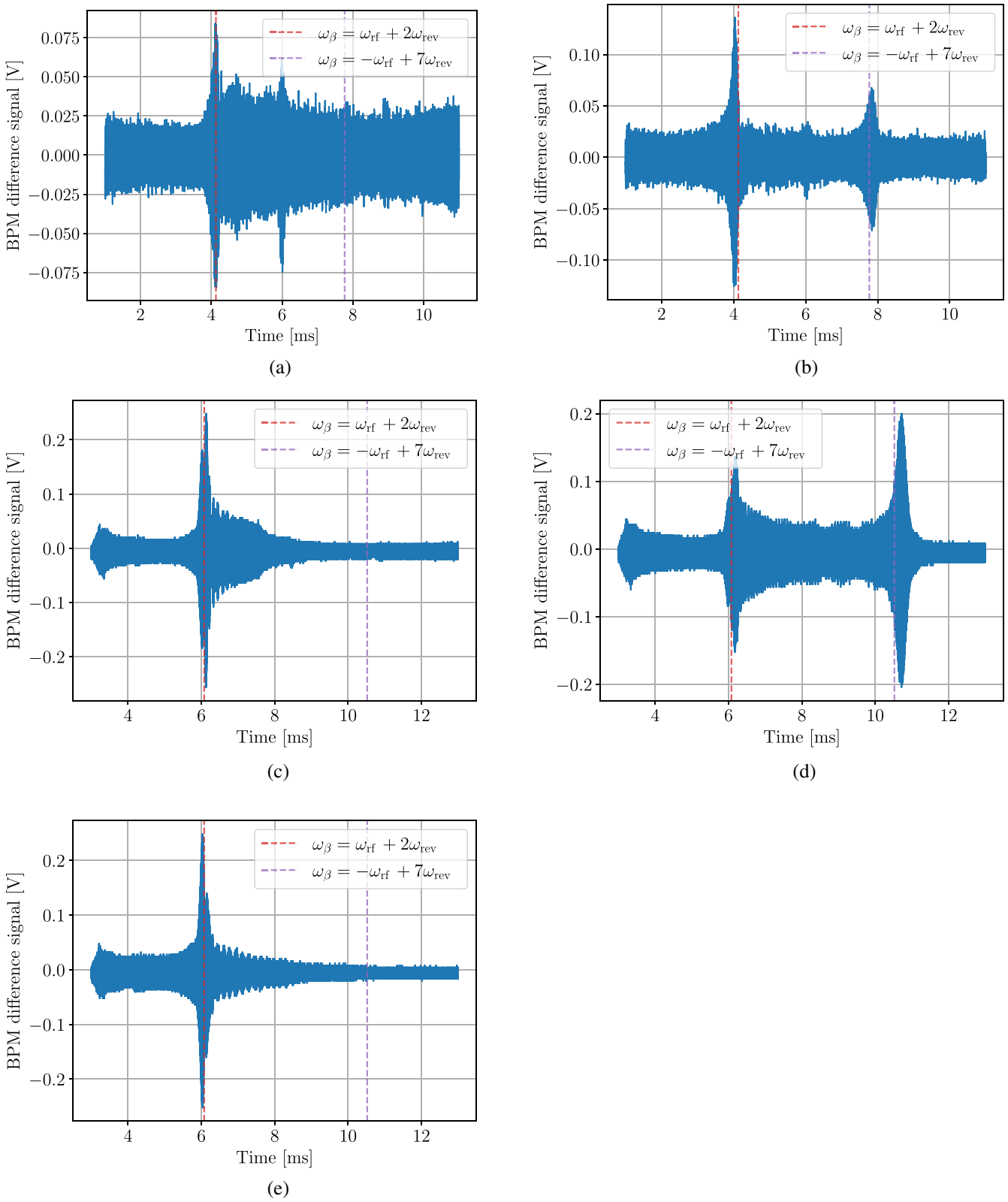

FIG. 14. Time domain data from beam position monitor difference signals showing how the oscillation triggered by rf knockout is mitigated/unmitigated depending on the arrangement of rf cavities. (a) $\Delta\theta/2\pi = 0.1$ mitigated (cavities 2 and 3), (b) $\Delta\theta/2\pi = 0.2$ unmitigated (cavities 2 and 4), (c) $\Delta\theta/2\pi = 0.3$ mitigated (cavities 7 and 4), (d) $\Delta\theta/2\pi = 0.4$ unmitigated (cavities 7 and 3), and (e) $\Delta\theta/2\pi = 0.5$ mitigated (cavities 7 and 2).

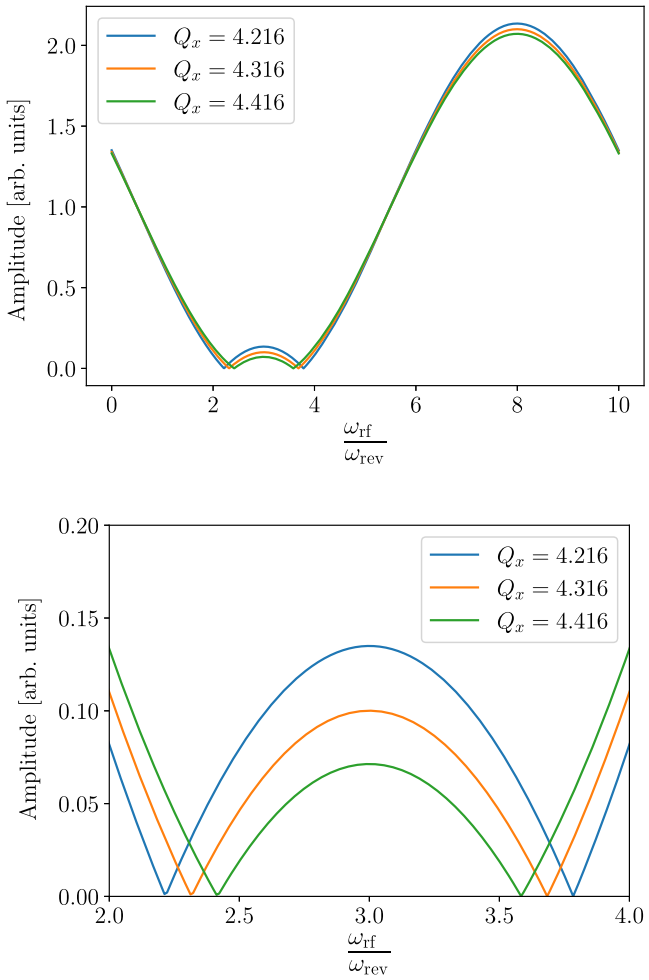

FIG. 15. Residual oscillation amplitude as a function of rf phase offset between cavities. Three horizontal tunes are shown. Details around the minima are also shown.

[1] S. Machida, S. Gallimore, B. Kirk, D. J. Kelliher, J.-B. Lagrange, C. T. Rogers, J. Pasternak, I. Gardner, R. Mathieson, T. J. Kuo, C. Hill, E. Yamakawa, D. Posthuma de Boer, and S. Sapkota, Fixed field alternating gradient accelerator (FFA) report, 2025, STFC Preprints:-62105376, http://purl.org/net/epubs/work/62105376.

[2] K. M. Terwilliger, L. W. Jones, and C. H. Pruett, Beam stacking experiments in an electron model FFAG accelerator, Rev. Sci. Instrum. **28**, 987 (1957).

[3] T. Uesugi, Y. Ishi, Y. Kuriyama, Y. Mori, C. Jolly, D. J. Kelliher, J.-B. Lagrange, A. P. Letchford, S. Machida, D. W. P. de Boer, C. T. Rogers, E. Yamakawa, and M. Topp-Mugglestone, Beam stacking experiment at a fixed field alternating gradient accelerator, Phys. Rev. Accel. Beams **28**, 012803 (2025).

[4] J. W. G. Thomason, The ISIS spallation neutron and muon source—The first thirty-three years, Nucl. Instrum. Methods A **917**, 61 (2019).

[5] K. R. Symon, D. W. Kerst, L. W. Jones, L. J. Laslett, and K. M. Terwilliger, Fixed-field alternating-gradient particle accelerators, Phys. Rev. **103**, 1837 (1956).

[6] T. Okawa, in *Proceedings of the Annual Meeting of JPS, unpublished* (1953).

[7] A. A. Kolomensky and A. N. Lebedev, *Theory of Cyclic Accelerators* (North-Holland, Amsterdam, 1966).

[8] K. M. Terwilliger, Radio frequency knockout of stacked beams, Report No. MURA-133, 1956.

[9] R. Baartman, FFAG04, Resonance crossing topics (2004), https://ffag2004.triumf.ca/programme.html.

[10] J. Le Duff, Integer resonance crossing in H.I. accumulator ring, eConf **C7910292**, 310 (1979).

[11] D. W. Kerst, Suppression of betatron oscillation excitation (RF knockout) by the RF accelerating system of a fixed field accelerator, MURA-215, 1957.

[12] L. W. Jones, C. H. Pruett, and K. M. Terwilliger, Experiments on radio frequency knockout of stacked beams, MURA-260, 1957.

[13] P. Barratt, I. Gardner, C. Planner, and G. Rees, RF system and beam loading compensation on the ISIS synchrotron, in *Proceedings of the 2nd European Particle Accelerator Conference* (1990), https://cds.cern.ch/record/963925.

[14] C. Jolly, D. J. Kelliher, J.-B. Lagrange, A. P. Letchford, S. Machida, D. W. Posthuma de Boer, C. T. Rogers, and A. Seville, Characterisation and mitigation of RF knockout during beam stacking—ISIS experimental data (2024), 10.5286/edata/957.